Journal of Molecular and Cellular Cardiology 194 (2024) 70–84

Contents lists available at ScienceDirect

Journal of Molecular and Cellular Cardiology

journal homepage: www.elsevier.com/locate/yjmcc

Transcriptional coactivation of NRF2 signaling in cardiac fibroblasts promotes resistance to oxidative stress

Lisa K. McClendon *, Rainer B. Lanz, Anil Panigrahi, Kristan Gomez, Michael J. Bolt, Min Liu, Fabio Stossi, Michael A. Mancini, Clifford C. Dacso, David M. Lonard *, Bert W. O'Malley *

Department of Molecular and Cellular Biology, Baylor College of Medicine, One Baylor Plaza, Houston, TX 77030, United States of America

ARTICLE INFO

Keywords:
Steroid receptor coactivator
NCOA1
NCOA2
NCOA3
Cardiac fibroblast
Oxidative stress
Cardiovascular diseases
Fibrosis

ABSTRACT

We recently discovered that steroid receptor coactivators (SRCs) SRCs-1, 2 and 3, are abundantly expressed in cardiac fibroblasts (CFs) and their activation with the SRC small molecule stimulator MCB-613 improves cardiac function and dramatically lowers pro-fibrotic signaling in CFs post-myocardial infarction. These findings suggest that CF-derived SRC activation could be beneficial in the mitigation of chronic heart failure after ischemic insult. However, the cardioprotective mechanisms by which CFs contribute to cardiac pathological remodeling are unclear. Here we present studies designed to identify the molecular and cellular circuitry that governs the anti-fibrotic effects of an MCB-613 derivative, MCB-613-10-1, in CFs. We performed cytokine profiling and whole transcriptome and proteome analyses of CF-derived signals in response to MCB-613-10-1. We identified the NRF2 pathway as a direct MCB-613-10-1 therapeutic target for promoting resistance to oxidative stress in CFs. We show that MCB-613-10-1 promotes cell survival of anti-fibrotic CFs exposed to oxidative stress by suppressing apoptosis. We demonstrate that an increase in HMOX1 expression contributes to CF resistance to oxidative stress-mediated apoptosis via a mechanism involving SRC co-activation of NRF2, hence reducing inflammation and fibrosis. We provide evidence that MCB-613-10-1 acts as a protectant against oxidative stress-induced mitochondrial damage. Our data reveal that SRC stimulation of the NRF2 transcriptional network promotes resistance to oxidative stress and highlights a mechanistic approach toward addressing pathologic cardiac remodeling.

1. Introduction

Transcriptional coactivators bind different transcription factors (TFs) and orchestrate TF-dependent activation of target genes. Steroid receptor coactivators (SRCs) are members of the p160 family of coactivators that govern transcriptional programs of not just nuclear receptors, but also many other TFs [1]. SRC functions have been linked to angiogenesis, immune response regulation, and cellular growth and regeneration. SRCs are ubiquitously expressed in many cell types [1,2], inclusive of fibroblasts, and have been shown to play important regulatory roles in mediating stromal cell functions [3], including in the heart.

We recently demonstrated that stimulation of SRCs with the small-molecule stimulator MCB-613 improves cardiac function after myocardial infarction (MI) and attenuates the chronic pathologic remodeling that ultimately leads to heart failure [4]. In mice, improved cardiac function was associated with a substantial 78% reduction in cardiac fibrosis. Mechanistically, we found that SRCs are highly expressed in CFs, and MCB-613 reduces inflammatory and pro-fibrotic signaling in CFs post-MI. These discoveries suggest that SRC activation in CFs may have therapeutic potential in the mitigation of chronic heart failure after infarction. The MCB-613 derivative, MCB-613-10-1, was designed as a more metabolically stable form [5]. Recently, we also have demonstrated that MCB-613-10-1 reduced pathogenic fibrotic remodeling by 28% after stroke in a rat model [5].

Cardiovascular disorders such as atherosclerosis, MI, myocardial ischemia/reperfusion, myocardial hypertrophy, and heart failure are all directly linked to oxidative damage resulting from intracellular production of reactive oxygen species (ROS) [6,7]. It has been established that ROS play pathophysiologic roles in CF activation and survival in both healthy and cardiovascular disease (CVD) states, including in the ischemic myocardium [7]. For example, ROS were shown to cause

* Corresponding authors.
E-mail addresses: Lisa.McClendon@bcm.edu (L.K. McClendon), rlanz@bcm.edu (R.B. Lanz), anil.panigrahi@bcm.edu (A. Panigrahi), kristan.gomez@bcm.edu (K. Gomez), michael.bolt@bcm.edu (M.J. Bolt), min.liu2@bcm.edu (M. Liu), stossi@bcm.edu (F. Stossi), mancini@bcm.edu (M.A. Mancini), cdacso@bcm.edu (C.C. Dacso), dlonard@bcm.edu (D.M. Lonard), berto@bcm.edu (B.W. O'Malley).

https://doi.org/10.1016/j.yjmcc.2024.07.001
Received 6 November 2023; Received in revised form 17 June 2024; Accepted 2 July 2024
Available online 4 July 2024

fibrosis by the production of a variety of profibrotic proteins [8,9], suggesting that oxidative stress may play a significant role in the pathophysiology of remodeling in the heart [10]. Ischemic injury causes a lack of glucose, oxygen, and nutrition, which results in cardiomyocyte necrosis. Unlike cardiomyocytes, CFs retain the ability to replicate in response to injury [11]. Beyond their role in the maintenance of structural integrity by synthesizing and remodeling the extracellular matrix (ECM), CFs are an important source of secreted factors [12] that contribute to orchestrating the progression from the initial inflammatory phase to scar tissue maintenance following MI [11,13]. Reduced fibrotic and inflammatory signaling in the surviving CFs at 24 h post-MI indicates that CF-derived signals are crucial contributors to cardioprotection [4].

The large number of signaling pathways involved in the development of cardiac fibrosis in vivo makes it difficult to pinpoint precise mechanisms underlying cardiac tissue response to MI. Characterizing the differential protein and gene expression in CFs is critical to better understand what CF responses are most important toward the cardioprotective effects of MCB-613-10-1. To achieve this, we performed cytokine profiling, whole transcriptome and proteomic analyses of CFs in response to MCB-613-10-1. Cytokine profiling shows MCB-613-10-1 inhibits the secretion of inflammatory and fibrotic proteins linked to fibrotic remodeling in CFs. Both transcriptional and proteomic profiling revealed key molecular and cellular pathways enriched for a pro-survival and anti-fibrotic phenotype. Given the robust induction of NRF2 pathway antioxidant genes and proteins, we evaluated the impact of MCB-613-10-1 on the susceptibility of CFs to oxidative stress. We provide original evidence that transcriptional regulation of antioxidant signaling in the absence of ROS provides CFs with the ability to resist oxidative stress. We show that MCB-613-10-1 promotes cell survival of anti-inflammatory CFs exposed to oxidative stress by suppressing apoptosis, and by protecting mitochondria from damage brought on by oxidative stress. Our results show that CF resistance to oxidative stress-mediated apoptosis is associated with an increase in HMOX1 expression through a mechanism involving SRC co-activation of NRF2, thereby protecting mitochondria and limiting inflammation and fibrosis.

2. Methods and materials

2.1. Animal procedures

Animal procedures were approved under our Institutional Animal Care and Use Committee (IACUC), using guidelines for the proper use of animals developed by the National Institutes of Health. Cardiac fibroblasts were isolated from female C57BL/6 wild type mice or B6.129 × 1-Nfe2l2tm1Ywk/J aged 8–10 weeks.

2.2. Cardiac fibroblast isolation

Cardiac fibroblasts were isolated following the protocol by Melzer, M et al., [14]. Cells were allowed to expand, trypsinized, counted and plated for experiments on day 4. All experiments were conducted using passage 1 CFs.

2.3. Cytokine assays

Cytokines in conditioned media from isolated CFs were detected using the Proteome Profiler Mouse XL Cytokine Array (R&D Systems) according to manufacturer's instructions.

2.4. CF Gel contraction assays

A 1:1 dilution of 150 μl of Type 1 rat collagen (Corning Cat. # 354236) with 150 μl culture media containing 75,000 CF cells were incubated in a 24-well culture plate. Gels were incubated at 37° C in a cell culture hood for 25 min. Gels were then dislodged from wells using a 30-gauge needle. 600 μl of media containing growth factors was added for 24 h. TGF-β (R&D Systems Cat. # 7666-MB-005) was used at 1 ng/ml as a positive control. Gel sizes were measured using ImageJ.

2.5. Phalloidin staining of collagen gels

Gels were fixed for 15 min in 4% paraformaldehyde (PFA) in PBS and stored in 0.16% PFA in PBS. Gels were cut into small pieces followed by blocking and permeabilization with 3% bovine serum albumin (BSA) in 0.2% Triton X-100 in PBS for 30 min. Gels were then washed 3 times for 7 min with 0.5% BSA and 0.03% Triton X-100 in PBS. Gels were then incubated with 1:400 Phalloidin antibody (ThermoFisher Cat. # A12379) and 1 μg/ml DAPI (Invitrogen Cat. # D1306) in 3% BSA and 0.2% Triton X-100 in PBS for 1 h. Gels were washed 3 times for 7 min and mounted on slides with 90% glycerol and sealed with fingernail polish.

2.6. Cell viability assay

The WST-1 cell proliferation assay measures the number of viable cells based on measurement of light absorbance resulting from mitochondrial succinate reductase's conversion of WST-1 to formazan. Cells were plated at 15,000 cells/well in a 96-well plate. CFs were treated with 600 μM hydrogen peroxide (H_2O_2) with and without MCB-613-10-1 or vehicle control as indicated. After 24 h of treatment, cell viability/mitochondrial metabolic activity was measured by WST-1 assay, according to the manufacturer's instructions (Roche Cat. # 501594401). Viability was reported as a percentage of cell viability compared to vehicle control.

2.7. Cell counts assay

Cells were plated in 24-well plates at 100,000 cells per well. CFs were treated with MCB-613-10-1 or vehicle control as indicated. Plates were imaged on a Sartorius Incucyte S3 imager for 17 h. Images were taken every hour.

2.8. Immunostaining

Five micron sections were cut and placed onto slides as previously described [4]. Immunofluorescence was performed by first removing the paraffin and then rehydrating the sections. After that, antigen retrieval was performed (EDTA, Diagnostic BioSystems, k038). Sections were permeabilized with 0.1% tween 20-PBS and 0.5% tween 20-PBS, blocked with 10% normal goat serum (NGS) in 0.1% tween 20-PBS, and then incubated with primary antibody in blocking solution Vimentin (1:50, AbCAM, ab92547) and HMOX1 (1:50, Proteintech, CL488–66743) followed by secondary (1:200, Invitrogen, A32740), and then DAPI (1:1000 Thermo Fisher Scientific Cat#62248). Fluorescence was counted from 3 images per high-powered field (HPF) from core and peri-infarct regions of each heart ($N = 3$ drug and $N = 3$ control) at 40× and quantified using CellProfiler. $N = 3$ control and $n = 3$ drug treated hearts at each time point. For cultured cells, cells were fixed in 4% formaldehyde for 10 min at room temperature. Primary antibodies HMOX1 (Abcam cat# ab13243) and NRF2 (Abcam cat# ab62352). Fluorescence was quantified using CellProfiler.

2.9. Apoptosis assay

Cells were plated in 96-well plates ($n = 6$ wells per condition). CFs were treated with MCB-613-10-1 or vehicle control as indicated. Cells were stained following the Cleaved Caspase-3 Staining Kit (FITC) (Abcam Cat# ab65613) manufacturer's protocol.

2.10. ROS detection assay

Cells were plated in 96-well plates at 15,000 cells per well ($n = 6$ per condition). CFs were treated with 600 μM H_2O_2 in the presence or absence of MCB-613-10-1 for 24 h. ROS was detected using the CellRox assay kit (Invitrogen Cat# C10422) according to manufacturer's instructions.

2.11. Cell painting assay

Cells were plated in 96-well plates (PerkinElmer PhenoPlate) at 7500 cells per well. After overnight incubation, cells were treated with vehicle control or MCB-613-10-1 for 24 h. The following day 900 μM H_2O_2 was added for 24 h. Cells were then stained live with MitoTracker Deep RED FM and Wheat Germ Agglutinin (Alexa Fluor 555) for 20 min at 37C. The stains were removed, and cells were then fixed with 4% paraformaldehyde at room temperature for 20 min. Following fixation, cells were washed 3 times in PBS at room temperature for 3 min each. Finally, cells were stained with DAPI, Concavalin A (Alexa Fluor 488), SYTO 14, and Phalloidin (Alexa Fluor 568) in a PBS solution containing 1% BSA and 0.1% TX-100 for 20 min. Cells were then washed 3 times with PBS at room temperature for 3 min each. Cells were left in PBS to image and imaged on a Yokogawa CV8000 spinning disk high throughput confocal microscope with max projections intensity images collected for each channel. Nine fields were collected per well. Images were analyzed using CellProfiler with DAPI used to segment the nucleus, and SYTO14 to segment the cytoplasm. Channel quantification occurred within these two regions. The number of nuclei (based on DAPI with a size threshold remove dead cells) per well were normalized to the average numbers of nuclei in the vehicle control wells to normalize differences in cell number between plates [15]. Nuclear eccentricity was calculated as the distance between foci of the ellipse and its major axis length. Higher eccentricity indicates a more elliptical shape. DAPI variance/mitochondrial variance is a measure of the variation of image intensity values. Uniform intensity (an object with the same pixel intensity across) would be 0. The higher the number, the higher range of pixel intensities. In H_2O_2, the DAPI and mitochondria signals have a wider range of intensities than the other treatments, which is commonly observed in stressed/dying cells. Mitochondrial contrast is determined as a measure of local variation in an image, indicating how much pixel intensities change in a small area containing mitochondria. In H_2O_2, mitochondria intensity changes highly within a small area, commonly observed in cells with mitochondrial dysfunction. Measurements were calculated according to CellProfilers instructions https://cellprofiler-manual.s3.amazonaws.com/CellProfiler-4.2.6/index.html.

2.12. Cell migration assays

Isolated CFs (passage 1) were plated at 150,000 cells per well in 24-well plates and incubated overnight. Wells were scratched with a 200 μl yellow pipette tip down the middle of each well. Cells were then washed with media with or without additional factors. Plates were imaged on a Sartorius Incucyte S3 imager for 46 h. Images were taken every 2 h.

2.13. RT-PCR

Cells were plated at 300,000 cells/ well in a 6-well plate and cultured overnight. Cells were treated with vehicle control or 6 μM MCB-613-10-1 for 4 or 24 h. RNA was isolated using the RNAeasy MiniKit (Qiagen Cat# 74106). For CF mRNA expression analysis, first-strand synthesis was performed using the SuperScript VILO MasterMix cDNA synthesis kit (ThermoFisher) per the manufacturer's instructions. Quantitative gene expression was performed using SYBR Green and gene-specific primers. Melt curves were performed for each primer set. Data were graphed relative to 18S ribosomal RNA internal standard using the ΔΔCt method.

2.14. Western blots

Primary C57BL6/J CFs or HeLa cells were seeded in 6-well plates at ~3.0×10^5 cells/well and allowed to settle overnight at 37 °C, 5% CO_2. The cells were treated with either 6 μM of MCB-613-10-1, 10 μM of MCB-613-10-1 or ethanol as vehicle control for 4 or 24 h. After treatment, the cells were rinsed with ice cold 1× PBS and scraped into a 1.5 ml centrifuge tube using 200 μl of RIPA buffer (Sigma Aldrich, Cat#: R0278) with protease/phosphatase inhibitor cocktail (100×) (Cell signaling, cat#: 5872S) at a 1:100 dilution. Cell lysates were incubated at 4 °C on a rocker for 45 min. The cell lysates were then spun down at 8000 *g* for 10 min at 4 °C and the supernatant was placed into clean tubes. Protein concentrations were measured using a BCA assay following the company's protocol (Thermo Fisher, cat# 23225). 20–30 μg of the protein sample were mixed with 4× Laemmli buffer (Bio-Rad, cat# 1610747) at a 1:3 dilution and heated for 5 min at 90 °C. Samples were loaded onto a 4–20% Tris-glycine gel (Bio-Rad, cat# 5671094) and run at 130 mV on a vertical electrophoresis cell (Bio-Rad, cat# 1656001) until the loading dye left the gel. The gel was transferred using a PDVF transfer kit (Bio-Rad, cat# 1704157) and the Transblot Turbo Transfer system. Gels were transferred for 7 min, and the membranes blocked with 5% non-fat dry milk TBST blotto (Bio-Rad, cat# 1706404). Membranes were then incubated with 3% non-fat dry milk TBST blotto and mixed with either anti-hmox-1 (Abcam, cat# 12343), anti-sqstm1 (Abcam, cat# ab91526), anti-KEAP1 (Cell Signaling, cat# 8047S), anti-SRC-1 (Cell Signaling, cat# 2191S), anti-SRC-2 (Cell signaling, cat# 96687S), anti-SRC-3 (Cell Signaling, cat# 2126S), or β-actin (Sigma, cat# A3854) and incubated overnight at 4 °C on a rocker overnight. The antibodies were all diluted at 1:1000 except for β-actin which was diluted at 1:50,000. After primary incubation, the membranes were washed with 1× TBST twice at 10-min intervals and twice at 5-min intervals. Secondary antibody was added to 3% non-fat dry milk TBST blotto at a 1:2000 dilution for 4 h at room temperature. The membranes were washed again with 1× TBST twice at 10-min intervals and twice at 5-min intervals. The membranes were developed using Prosignal™ Femto (Promethus, cat# 20–302) for 2 min and images were taken using the Biorad Chemidoc™ MP imaging system.

2.15. RNA-Seq

RNA sequencing was performed using Illumina platforms located at Novogene (Durham, NC). Total RNA extracted from mouse primary CFs (provided in triplicates) were incubated with poly-T oligo-attached magnetic beads to isolate mRNA. cDNA synthesis was carried out using random hexamer primers for reverse transcription and dTTP for the second strand cDNA synthesis. Library construction included cDNA end repair, A-tailing, adapter ligation, size selection, amplification, and purification, followed by Qubit fluorometric quantification, real-time PCR for quantification and bioanalyzer analysis for size distribution detection. Sequencing raw data controls followed Novogene's in-house procedures, paired-end clean reads were aligned to the mouse reference genome mm39 using Hisat2 v2.0.5; statistics of sequencing quality and mapping for all samples were: error rate 0.02, Q Phred value Q20 > 97.6, Q30 > 93.7, total reads >65 million, proper mapping >88.5%, Read distribution: >95% exonic, <5% intronic, <3% intragenic. Counts v1.5.0-p3 was used to count the reads numbers mapped to each gene, and FPKM of each gene was calculated based on read count mapped to the gene and the length of the gene. DESeq2 was used for calculating differential expression values; the resulting *P*-values were adjusted using Benjamini and Hochberg's approach for controlling the false discovery rate. Genes with an adjusted *P*-value ≤0.05 found by DESeq2 and thresholded 1.5× (4 h samples) and 2× (24 h samples) fold change in normalized expression were assigned as differentially expressed genes (DEGs).

Gene ontogeny overrepresentation analyses were done using the public on-line resources PANTHER knowledgebase v17.0 (https://www.

pantherdb.org), DAVID Knowledgebase v2023q2 (https://david.ncifcrf.gov), and GSEA/MSigDB (https://www.gsea-msigdb.org/gsea/msigdb/index.jsp) using individual data resources such as GO, KEGG and Reactome, independently.

2.16. Proteome profiling

Protein extraction, digestion and peptide fractionation was carried out based on the protocol adapted from [16]. Cells were lysed in 8 M urea buffer, reduced/alkylated and digested using LysC and Trypsin proteases. 100 μg peptide per sample were labeled with TMT10 plex isobaric label reagent (Thermo Fisher Scientific) according to manufacturer's protocol. The high-pH offline fractionation was carried to generate 24 peptide pools and acidified with final concentration of 0.1% formic acid (FA). The deep-fractionated peptide samples were separated on Vanquish Neo UHPLC (Thermo Fisher Scientific, San Jose, CA) system coupled to Orbitrap Eclipse (Thermo Fisher Scientific, San Jose, CA). The samples were loaded on Pepmap Neo trap (5μmX300μmX5mm, C18) switched in-line with an in-housed 20 cm x 75μmI.D. column (Reprosil-Pur Basic C18, 1.9 μm, Dr. Maisch GmbH, Germany). Peptide elution was done using a 110 min discontinuous gradient of 80% acetonitrile buffer (B) in 0.1% formic acid at 250 nl/min (2–35%B: 87 min, 35–60%B: 10 min, 60–95%B: 7 min, 95–50%B: 6 min). The heated column was maintained at 60 °C. The eluted peptides were directly electro-sprayed into mass spectrometer operated in the data-dependent acquisition mode acquiring HCD fragmentation spectra with a 2 s cycle time. The MS1 was done in Orbitrap (120,000 resolution, scan range 375-1500 *m/z*, 50 ms Injection time) followed by MS2 in Orbitrap at 30000 resolution (HCD 38%) using the TurboTMT algorithm. Dynamic exclusion was set to 20 s, and the isolation width was set to 0.7 m/z. The data search was conducted using the mouse protein database downloaded from GENCODE (release 32). The MS data search and analysis pipeline was previously described [17].

2.17. ChIP-qPCR assays

Primary female C57BL6/J CFs were plated in 10-cm dishes at ~1.5 × 10^6 cells/plate and allowed to settle overnight at 37 °C, 5% CO_2. The cells were then treated with either 6 μM MCB-613-10-1 or ethanol vehicle control for four hours. After treatment, the cells were fixed, and nuclei were prepped for sonication according to the Covis shearing kit protocol (Covaris, Cat# 520154). The cell suspension was sonicated using a Covaris Ultrasonicator LE220 for 17 min with settings recommended by the Covaris shearing kit protocol. After sonication, chromatin fragment size was verified by agarose gel electrophoresis and was found to be around 200 bp–500 bp. Immunoprecipitation of the cross-linked protein/DNA was done using the EZ ChIP kit (Millipore, Cat # 17–371). The samples were mixed with either IgG control, anti-NRF2 (Cell Signaling Cat # D1Z9C), anti-SRC-1 (Cell Signaling, Cat# 128E7), anti-SRC-2 (Cell Signaling, Cat# D2X4M), or anti-SRC-3 (Cell Signaling, Cat # 2126S) and incubated at 4 °C on a rocker overnight. The antibodies were added according to the recommended dilutions for ChIP assays by the manufacturer. After the protein/DNA complexes were pulled, washed, and reverse cross-linked according to the EZ ChIP protocol, the DNA was purified using the QIAquick PCR purification kit (Qiagen, Cat #28104). The DNA samples were eluted with 50 μl of water (Invitrogen). Real-time PCR was performed using the following primers within the Hmox1 5′ upstream region: E1: 5′ GGG CAG TCT TAA GCA ATC CA −3′, and 5' CCA TGA CTC AGC GAA AAC AG-3′, E2: 5' CCT AGT GCA GAA GGC TTT GG-3′, and 5' TCA GGG GAA GAA CAA AGG AA-3′, P1: 5' GCT GGA ATG CTG AGT TGT GA-3′ and 5′ TGA GGG AAC AGA GGG TGA CT-3′, E3: 5' GCT GGA ATG CTG AGT TGT GA-3′, and 5′ TGA GGG AAC AGA GGG TGA CT −3′. For qPCR, samples were diluted 1:2 and inputs were diluted 1:20 with water (Invitrogen) and 2 μl of the diluted material was used for PCR reactions.

2.18. Seahorse assay

Primary female CFs were seeded at 25,000/well on the 96-well plate provided in the Seahorse XFe assay kit (Agilent, 103,798–100) and allowed to settle overnight in the CO_2 incubator. The cells were treated with either 6 μm MCB-613-10-1 or ethanol and incubated for 24H. Meanwhile, the cartridge was hydrated with distilled water at 37 °C without CO_2 overnight. The water was removed from the cartridge and seahorse calibration reagent (Agilent, 100,840–000) was added and put back in the non-CO_2 37 °C incubator 1 h prior to the assay. Drugs from the mitochondrial stress kit (Agilent,103,010–100) were diluted with fresh XF media supplemented with 25 mM glucose, 10 mM pyruvate, 10 mM of glutamine (Agilent, 103,680–100). The cells were washed twice and 180 μl of supplemented XF media was added to the plate and put into a non-CO_2 incubator for 1 h prior to the assay. 20 μl of each drug was placed into their respective chambers in the hydrated cartridge making a final concentration of 1 μM Oligomycin, 1.0 μM FCCP, and 0.5 μM Rotenone/ Antimycin A. After calibration, the plate was read using the Seahorse XFe96 analyzer (Agilent, S7800A) in the Mouse Metabolism and Phenotyping Core.

2.19. Statistics

Results are reported as the mean +/− SEM. The statistical significance of the difference between means was assessed using Prism Software using the paired 2-tailed Student's *t*-test. *P* values of <0.05 were considered significant.

3. Results

3.1. MCB-613-10-1 suppresses secretion of proteins associated with fibrotic remodeling in CFs

In our recent study, we discovered that MCB-613-10-1 led to an increase in resident CF numbers 24 h after MI, which was followed by the appearance of cartilage oligomeric matrix protein positive fibroblasts associated with improved structural integrity at 12 weeks [4]. At 24 h post-MCB-613-10-1 treatment, the surviving CFs showed reduced fibrotic and inflammatory signaling, indicating that CF-derived signals constitute an important component of cardioprotection. To identify cytokines associated with an improved response to injury, cytokines were measured in conditioned media from isolated CFs treated with MCB-613-10-1 compared to control. CFs treated with MCB-613-10-1 present a unique CF secretory signature (Fig. 1A and B). Of the ones examined, no secreted proteins were increased in response to MCB-613-10-1 treatment. In contrast, Insulin-like growth factor-binding protein 2 (IGFBP2), Osteoprotegerin (OPG), C—C motif chemokine ligand 2 (CCL2), Cystatin C, Transferrin (TF), WNT1-inducible-signaling pathway protein 1 (WISP1), chemokine ligand (CXCL)16, and CXCL12 were decreased in CFs treated with MCB-613-10-1, as were the mRNA levels of *Wisp1*, *Ccl2*, *Opg*, matricellular proteins thrombospondin 2 (*Thbs2*) and cellular communication network 3 (*Ccn3*) (Fig. 1C) and protein levels of TF and CCL2 (Fig. 1D). These results indicate that SRC activation impacts cardiac fibroblast expression of cytokines and chemokines. These findings also reveal a novel observation that SRC activation controls expression of nonstructural ECM-associated signaling proteins that may govern protective cardiac fibrotic remodeling.

3.2. MCB-613-10-1 inhibits CF activation

To determine whether MCB-613-10-1 alters activated CF functions, gel contraction, migration and proliferation were measured in CFs isolated from mice. Functional studies show that MCB-613-10-1 blocks basal and TGF-β-induced fibroblast collagen I gel contraction (Fig. 2A). We observed the effects of MCB-613-10-1 on F-actin skeleton morphology by performing phalloidin staining (Fig. 2C). The results

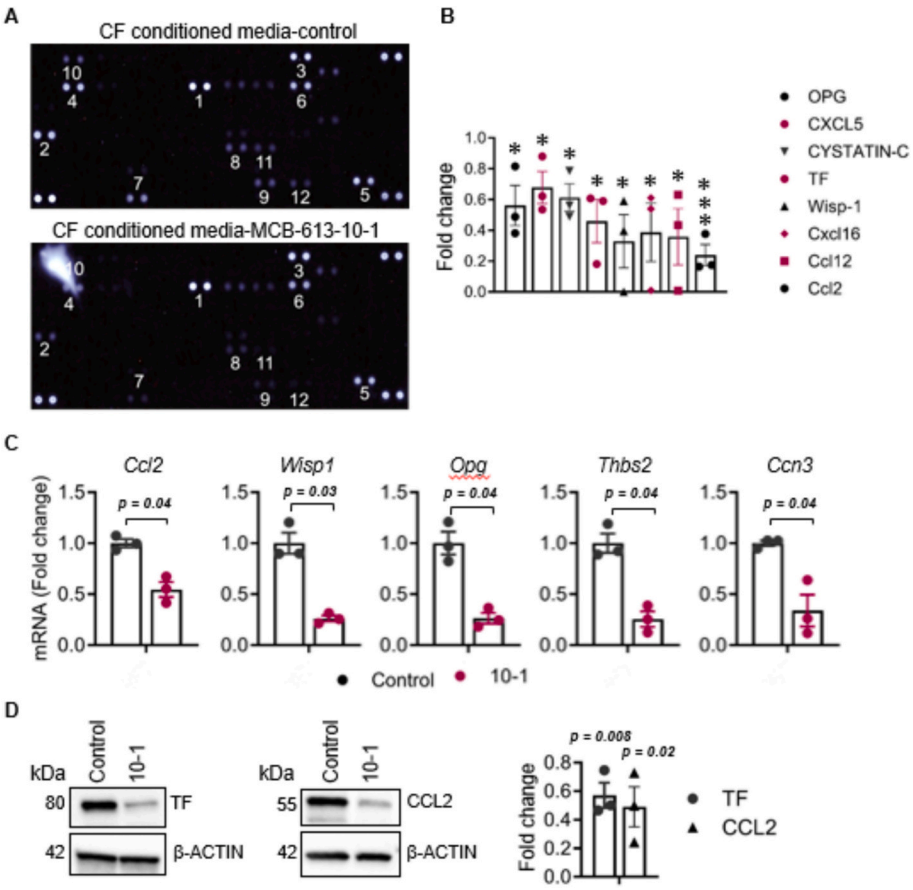

Fig. 1. SRC activation decreases cytokines and matricellular proteins associated with fibrotic remodeling in cardiac fibroblasts. (a) Analysis of secreted cytokine factors in conditioned media from control or MCB-613 10–1–treated cardiac fibroblasts (6 μM for 24 h) using R&D Systems Proteome ProfilerTM Antibody Array. (b) Array quantification. * ≤ 0.05, ** ≤ 0.01, *** 0.001. (c) Validation of mRNA expression by RT-PCR of cultured cells for *Ccl2*, *Opg* and matricellular genes*Thbs2* and *Ccn3*. Representative values from 3 separate experiments. Values shown are mean ± SEM; Student's *t*-test $n = 3$ control and $n = 3$ 10–1. (d) Representative Western blots for TF and CCL2 and quantification of 3 experiments.

suggest that SRCs prevent actin polymerization and actin cytoskeleton remodeling, which may be associated with the promotion of focal adhesion turnover and cell migration [30]. Furthermore, after treatment with transforming growth factor TGF-β, filamentous F-actin was significantly enhanced, and this effect was inhibited by pretreatment with MCB-613-10-1 (Fig. 2B). This result further illustrates that F-actin polymerization depends on MCB-613-10-1 treatment. Cell migration was assessed as another stress-related function of CFs. Cell migration was suppressed 22 h after MCB-613-10-1 treatment indicating that MCB-613-10-1 inhibits CF migration (Fig. 2C). Next, we investigated if MCB-613-10-1 limits cell viability, cell numbers or apoptosis which may affect gel contraction and cell migration. The WST-1 assay is based on the cleavage of tetrazolium salt to formazan by cellular mitochondrial dehydrogenase. In addition to measuring cell viability, the WST-1 assay also provides a measure of mitochondrial metabolic function. Cell viability was slightly increased in CFs following 6 μM MCB-613-10-1 treatment and further increased with 10 μM of MCB-613-10-1 indicating that the SRC stimulator does not decrease cell viability (Fig. 2D). These findings suggest that MCB-613-10-1 stimulates mitochondrial metabolism. Cell numbers were initially decreased in isolated CFs but recovered and proliferated in non-treated cells while MCB-613-10-1 treated CFs did not proliferate (Fig. 2D), but apoptosis was not increased (Supplemental Fig.1). These findings indicate that MCB-613 inhibits CF proliferation while enhancing cell viability without inducing CF apoptosis. We next measured SRC protein expression in response to MCB-613-10-1 in CFs to determine if there is an association between SRC protein expression and CF activation. We found that treatment with MCB-613-10-1 did not result in a change in SRC expression, indicating that CF activation likely correlates with SRC activation and function, but not coactivator abundance (Fig. 2E).

3.3. SRC activation stimulates the NRF2 transcriptional network in cardiac fibroblasts and improves mitochondrial function

RNA-seq was performed to identify SRC transcriptional regulatory mechanisms involved in the cardioprotective response to MCB-613-10-1. To focus on early transcriptional targets compared to later phenotype-related gene expression, RNA was isolated from primary CFs following treatment with MCB-613-10-1 or control at 4 and 24 h, respectively. We next analyzed differentially expressed genes (DEGs). At 4 h, 191 genes were differentially up-regulated and 230 genes down-regulated in MCB-613-10-1 treated CFs compared to vehicle control (Supplemental Fig. 2). Unbiased gene ontology and gene network analyses revealed the top over-represented GO terms included cell cycle, mitosis, chaperone, protein folding, and cellular response to fibroblast growth factor stimulus (Supplemental Fig. 3). Bioinformatic pathway analysis of differentially expressed genes at 4 h revealed that MCB-613-10-1 modulation of the fibroblast transcriptional response was dominated by the NRF2 pathway and nuclear receptors meta-pathway followed by cell cycle, VEGFA-VEGFR2 signaling, and the MAPK signaling pathway (Fig. 3A, left panel). Upregulation of NRF2 signaling pathway genes and NRF2 target genes at 4 h (Supplemental Fig. 3) indicates MCB-613-10-1 induces the NRF2 transcriptional network.

Next, we performed bioinformatic analysis of at least two-fold

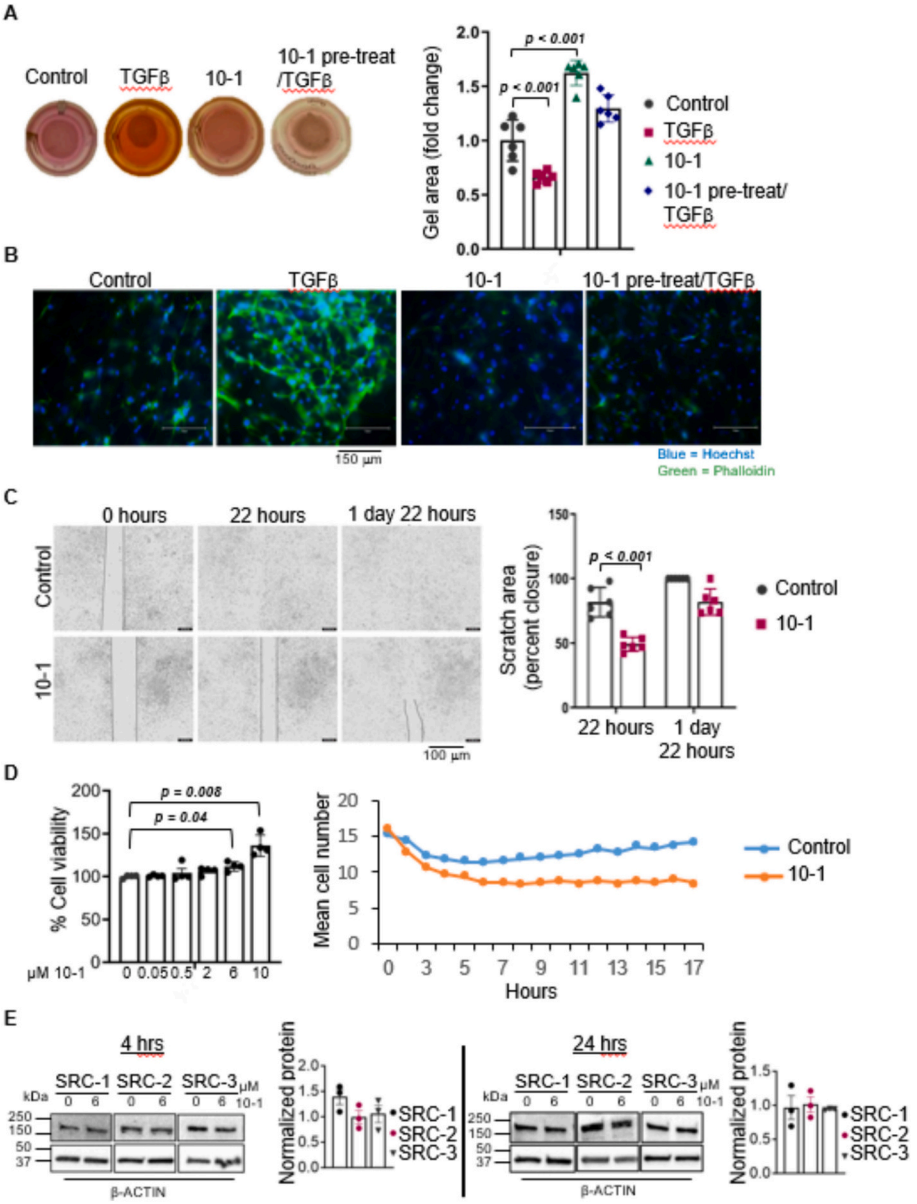

Fig. 2. 10–1 inhibits cardiac fibroblast activation. (a) CFs were cultured in a collagen I gel and treated with TGF-β or MCB-613-10-1. Gel size was measured using ImageJ. Representative images of 6 experiments with 6 wells per experiment. (b) Representative images of cells growing in collagen I gels were treated with TGF-β or pre-treated with 10–1 then stained with phalloidin and imaged. (c) Cell migration was measured using a scratch assay. Images were taken at different time points. Quantification of the percent closure of the scratch area. Representative images from 3 experiments. Values shown are mean ± SEM; Student's *t*-test $n = 6$ control and $n = 6$ 10–1 from one experiment. (d) CF cell viability was measured at 24 h. Values shown are mean ± SEM; Student's t-test $n = 4$ from one of three experiments. Mean cell counts were measured every hour for 17 h. Representative of two experiments. (e) Representative images of SRC-1, 2 and 3 protein expression in cultured cardiac fibroblasts 4 and 24 h after MCB-613-10-1 treatment. Quantification of 3 experiments.

differentially expressed genes at 24 h. At 24 h, 1084 genes were differentially up-regulated and 1167 genes down-regulated in MCB-613-10-1 treated CFs compared to vehicle control (Supplemental Fig. 2), indicating that MCB-613-10-1 triggers more transcriptional changes at 24 h compared to 4 h. The top GO terms associated with the 24-h transcriptional response included cell cycle, proteosome, extracellular matrix, endoplasmic reticulum, and DNA repair (Supplemental Fig. 3b). Genes associated with the GO term extracellular matrix were predominantly down-regulated (Supplemental Fig. 4), supporting our findings here and in previous studies [4,5]. In addition to the novel finding of SRC activation leading to downregulation of matricellular genes shown in Fig. 1, the cardiac ECM remodeling-Lysyl oxidase (*Lox*) and 3 lox-like isoenzymes (*Lox1*, *Lox2* and *Lox3*) [18] were highly down-regulated in response to MCB-613-10-1 in CFs at 24 h (Supplemental Fig. 4), indicating that MCB-613-10-1 regulates secreted non-structural ECM signaling proteins. Top signaling pathways associated with the 24-h upregulated transcriptional response genes included cellular responses to stimuli, cell cycle-related signaling and KEAP1-NRF2 pathway and nuclear events mediated by NRF2 (NFE2L2) (Fig. 3A, right panel). Consistent with 4-h transcriptome data, KEAP1-NRF2 signaling pathway genes also were predominantly upregulated at 24 h (Supplemental Fig. 3), indicating that SRC activation stimulates the NRF2 transcriptome by liberating NRF2 from being hedged in the cytoplasm. Given that the NRF2 pathway was the top and 4th overrepresented pathway at 4 and 24 h respectively, we performed a comparative evaluation of all DEGs in the NRF2 pathway at 4 and 24 h (Fig. 3 and Supplemental Figs. 5–7). DEGs at 4 h predominantly encode antioxidant proteins and the category of "other" consisting of key NRF2 target genes

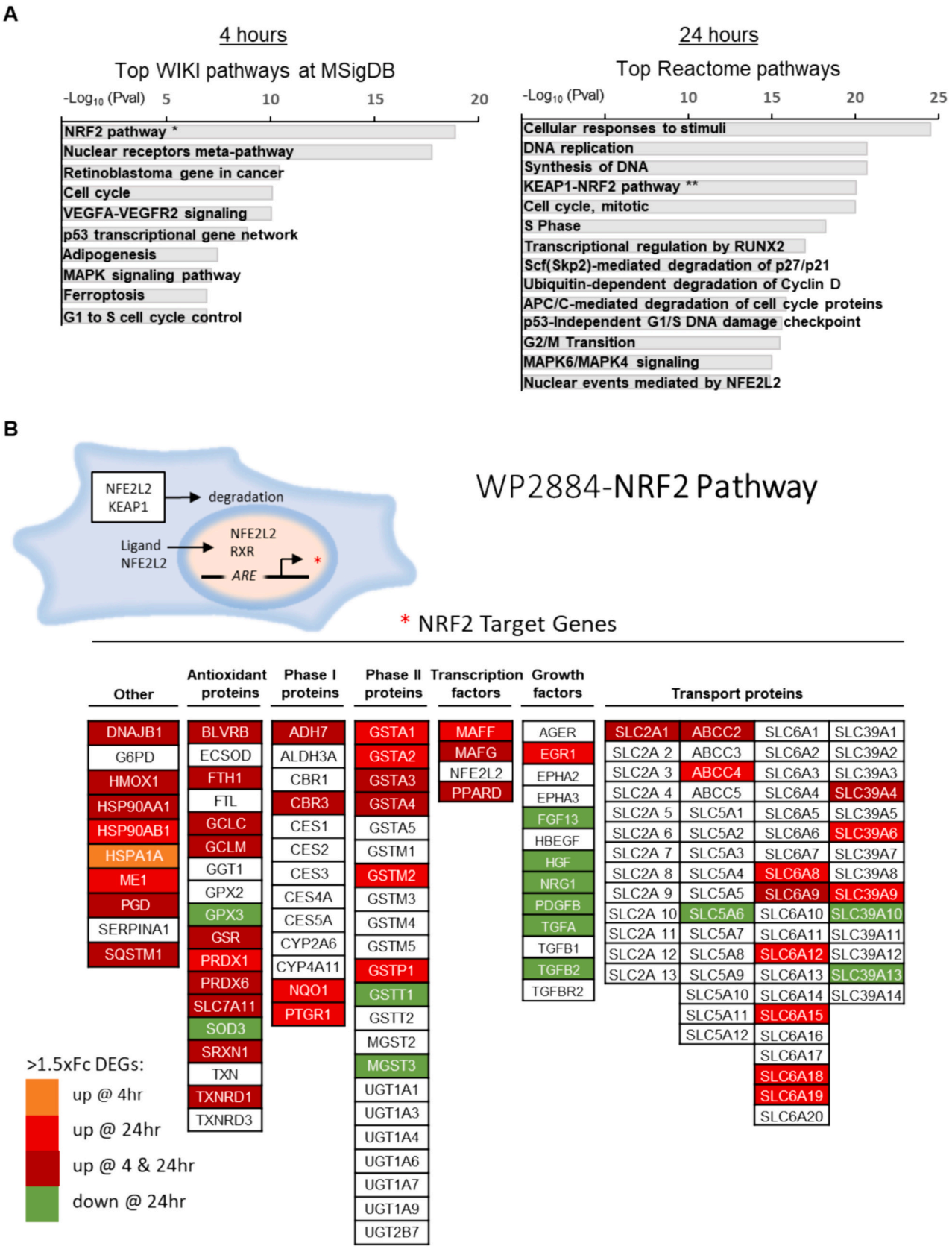

Fig. 3. Analysis of the SRC activation gene signature in CFs shows the cardioprotective transcriptional response is dominated by the NRF2 transcriptional network. (a) Gene ontology analysis of functional annotation clusters and molecular pathways of differentially regulated genes 4 and 24 h after 10–1 treatment in cardiac fibroblasts compared to vehicle control. (b) Differentially expressed genes in NRF2 pathway at 4 and 24 h following 10–1 treatment.

Heme oxygenase 1 (*Hmox1*) and Sequestosome 1 (*Sqstm1*) compared to phase 2 proteins and transport proteins suggesting that MCB-613-10-1 stimulates antioxidant genes in the NRF2 transcriptional network compared to transport proteins. Interestingly, almost 50 % of the NRF2 growth factor targets were downregulated at 24 h indicating decreased cellular growth factor signaling. In contrast to HSPA1A, which is only upregulated at 4 h, genes upregulated at 4 h were also upregulated at 24 h. Nineteen NRF2 pathway genes were exclusively up regulated in response to MCB-613-10-1 at 24 h, in line with a more robust transcriptional response at 24 h.

Next, to validate MCB-613-10-1-induced gene expression, we measured the transcriptional response for NRF2-related signaling pathway genes in control and MCB-613-10-1-treated CFs. RT-qPCR data show that the NRF2-target genes *Hmox1*, *Nqo1*, *Gsta3*, *Sqstm1* and *Prdx1* were up-regulated at both 4 and 24 h after MCB-613-10-1 treatment (Fig. 4A). We measured protein expression of NRF2 target gene HMOX1, SQSTM1 and the NRF2 negative regulator Kelch-like ECH-associated protein 1 (KEAP1) in cell lysates from CFs treated with vehicle control compared to MCB-613-10-1 for 4 and 24 h. HMOX1 and SQSTM1 proteins were increased in response to MCB-613-10-1 at both 4 and 24 h (Fig. 4B) and KEAP1 protein was decreased only at 24 h. To directly confirm the activation of NRF2, quantification of NRF2 nuclear proteins was measured by NRF2 immunofluorescence staining. MCB-613-10-1 increased the fluorescent intensity of nuclear NRF2 (Fig. 4C). We also evaluated HMOX1 expression by immunostaining. HMOX1 staining was more abundant in response to MCB-613-10-1 (Fig. 4C). In further support of NRF2 activation, cell fractionation of cytoplasmic fractions compared to nuclear cellular protein fractions shows nuclear accumulation of NRF2 following 24 h MCB-613-10-1 treatment (Fig. 4D). Given the role NRF2 in respiration [19], we evaluated the effect of MCB-613-10-1 on oxygen consumption, as a measure of mitochondrial function, in intact CFs. Compared to control, oxygen consumption in drug-treated

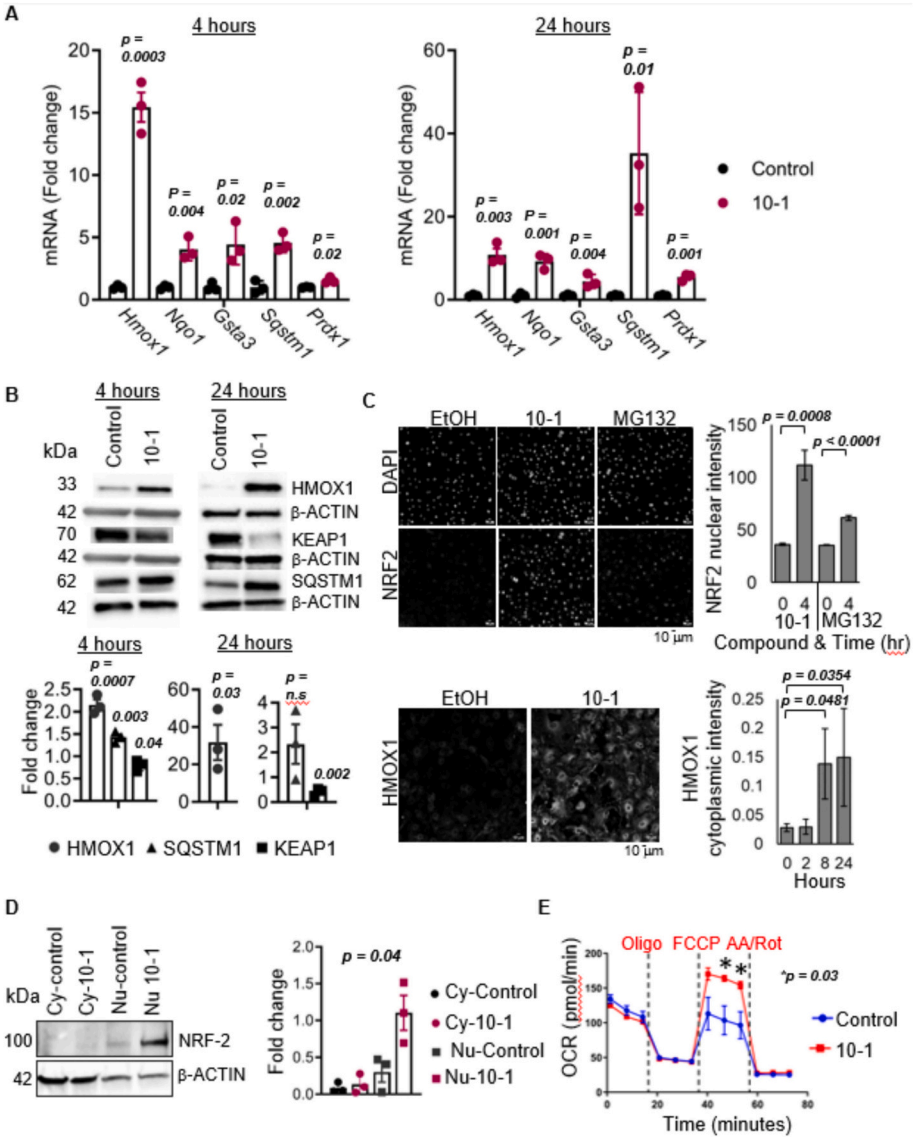

Fig. 4. 10–1 stimulates the NRF2 oxidative stress cellular defense pathway and improves mitochondrial function. RT-PCR and Western Blot validation of RNAseq 4 and 24-h following treatment for (a) RT-PCR for NRF2 antioxidant response genes at 4- and 24-h control or 10–1 treatment. Values shown are mean ± SEM; Student's *t*-test $n = 3$ control and $n = 3$ 10–1. Representative of 3 experiments. (b) Western Blots for NRF2 antioxidant response proteins at 4- and 24-h control or MCB-613-10-1 treatment. (c) NRF2 and HMOX1 immunostaining at 4 h. The positive control MG132 induces nuclear localization of NRF2. Representative images of 3 experiments. Quantification of HMOX1 in 5 images per condition. (d) Western Blot of NRF2 in cytoplasmic and nuclear fractions in WT CF lysates. (e) Seahorse analysis of cellular oxygen consumption rate (OCR) in CFs treated with 10–1 compared to control. Data are representative of 3 independent experiments. $n = 4$ measurements per treatment group.

CFs was increased (Fig. 4E), demonstrating MCB-613 improves mitochondrial function by enhancing energy metabolism.

Given the robust changes in NRF2 pathway proteins, we performed quantitative proteomics. Protein was isolated from primary CFs following treatment with MCB-613-10-1 or control at 24 h. Tandem mass tag (TMT) proteomics profiling of CFs treated with MCB-613-10-1 and analyzed against mock-treated CFs for differential iBAQ (peptide area-based quantification) for the most part reproduced the differential expression profile we obtained by RNA-seq. 410 proteins satisfied thresholding at 1.5×-fold change presence and Padj <0.05 significance (Supplemental Fig. 8). 248 of these proteins agreed with differentially expressed genes called at 1.5×-fold change, 204 (82%) of which also agreed with the direction of expression change. Statistical over-representation tests carried out with the differential proteins alone or

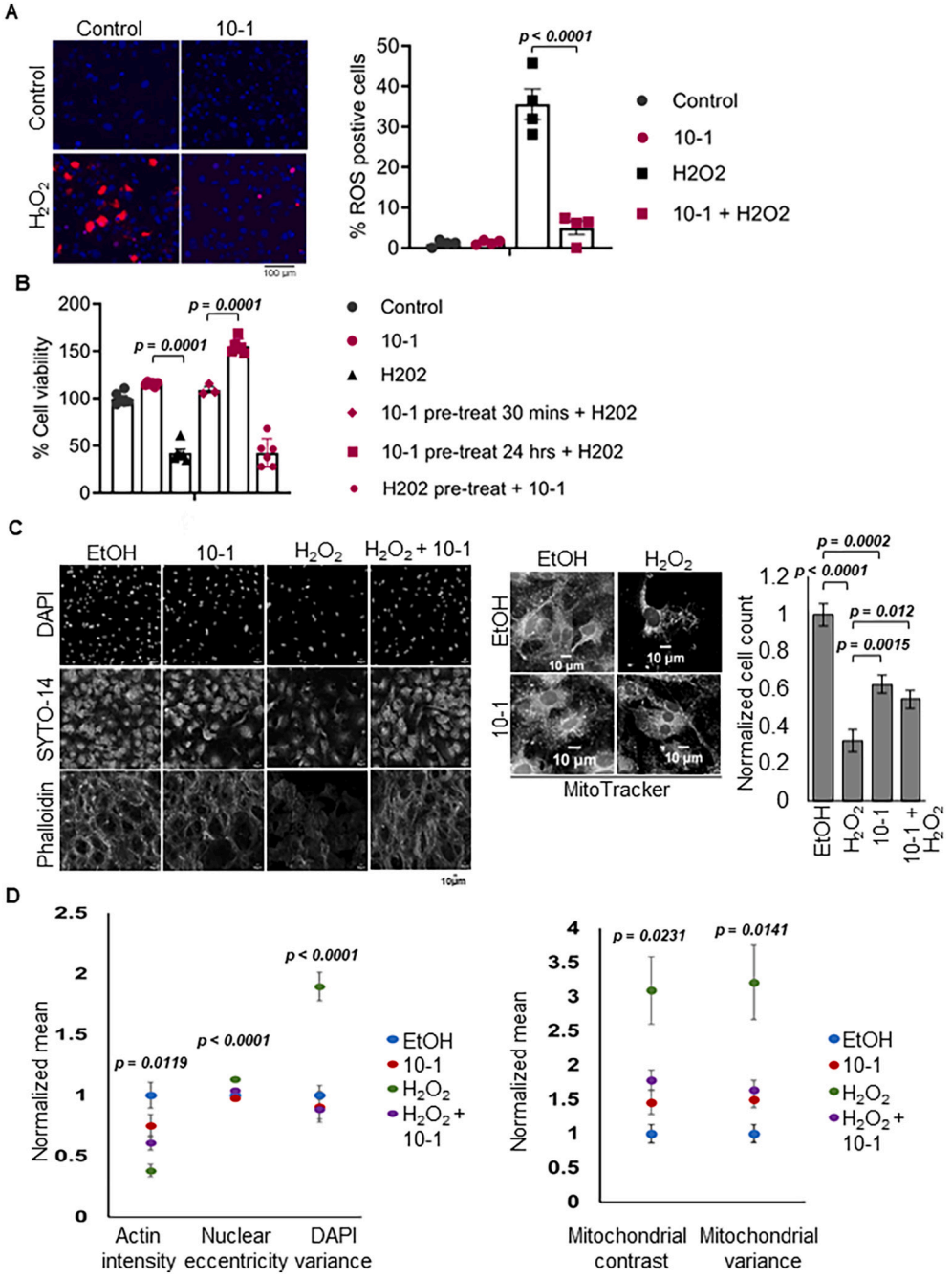

Fig. 5. MCB-613-10-1 prevents production of intracellular ROS and promotes resistance to H_2O_2 -induced loss of cell numbers and cellular and mitochondrial dysfunction (a) CFs were treated with 600 μM H_2O_2 in the presence or absence of MCB-613-10-1 for 24 h. Intracellular ROS was detected using the CellRox assay. Representative images from 3 experiments $n = 6$ control and $n = 6$ MCB-613-10-1. Quantification of 4 fields of view for percent ROS positive cells (right panel). (b) Cell viability was measured 24 h following addition of 600 μM H_2O_2 with 30-min 10–1 (6 μM) pre-treatment, 24-h 10–1 pre-treatment or 6 h H_2O_2 pre-treatment followed by 24 h 10–1. Values shown are mean ± SEM; Student's *t*-test. $n = 6$ for each condition representative of three experiments. (c) Cell painting was performed on CFs that were pre-treated with MCB-613-10-1 for 24 h followed by 900 μM H_2O_2 or no H_2O_2. Representative images from 3 experiments. Quantification of two experiments $n = 4$ for each experiment. Values shown are mean ± SEM; Student's t-test for H_2O_2 compared to H_2O_2 plus MCB-613-10-1. (d) Cell painting analysis of cellular and mitochondrial features. Quantification of two experiments, $n = 4$ replicates for each experiment. Values shown are mean ± SEM; Student's t-test for H_2O_2 compared to H_2O_2 plus MCB-613-10-1.

with their intersection with the 1.5×-Fc DEGs reproduced the NRF2-related enrichments (Supplemental Figs. 9 & 10) – along with the differential protein expression for the top enrichment (Supplemental Fig. 11), including the DAVID WIKI overrepresentation analysis generated with the 248 shared proteins and DEGs. These results establish that the NRF2 pathway is the dominant pathway stimulated by MCB-613-10-1 in cardiac fibroblasts.

3.4. MCB-613-10-1 promotes cell survival and preserves cellular and mitochondrial morphology and function following H_2O_2 exposure

Given the role of NRF2 in cell migration, proliferation and ROS control in ischemic cardiovascular disease [20], we evaluated the effect of MCB-613-10-1 on ROS production. To ascertain if MCB-613-10-1 influences H_2O_2-mediated oxidative stress in cardiac fibroblasts, CFs were exposed to H_2O_2 to induce the generation of intracellular ROS. MCB-613-10-1 alone did not lead to accumulation of ROS by itself. Intracellular ROS was robustly inhibited in the presence of MCB-613-10-

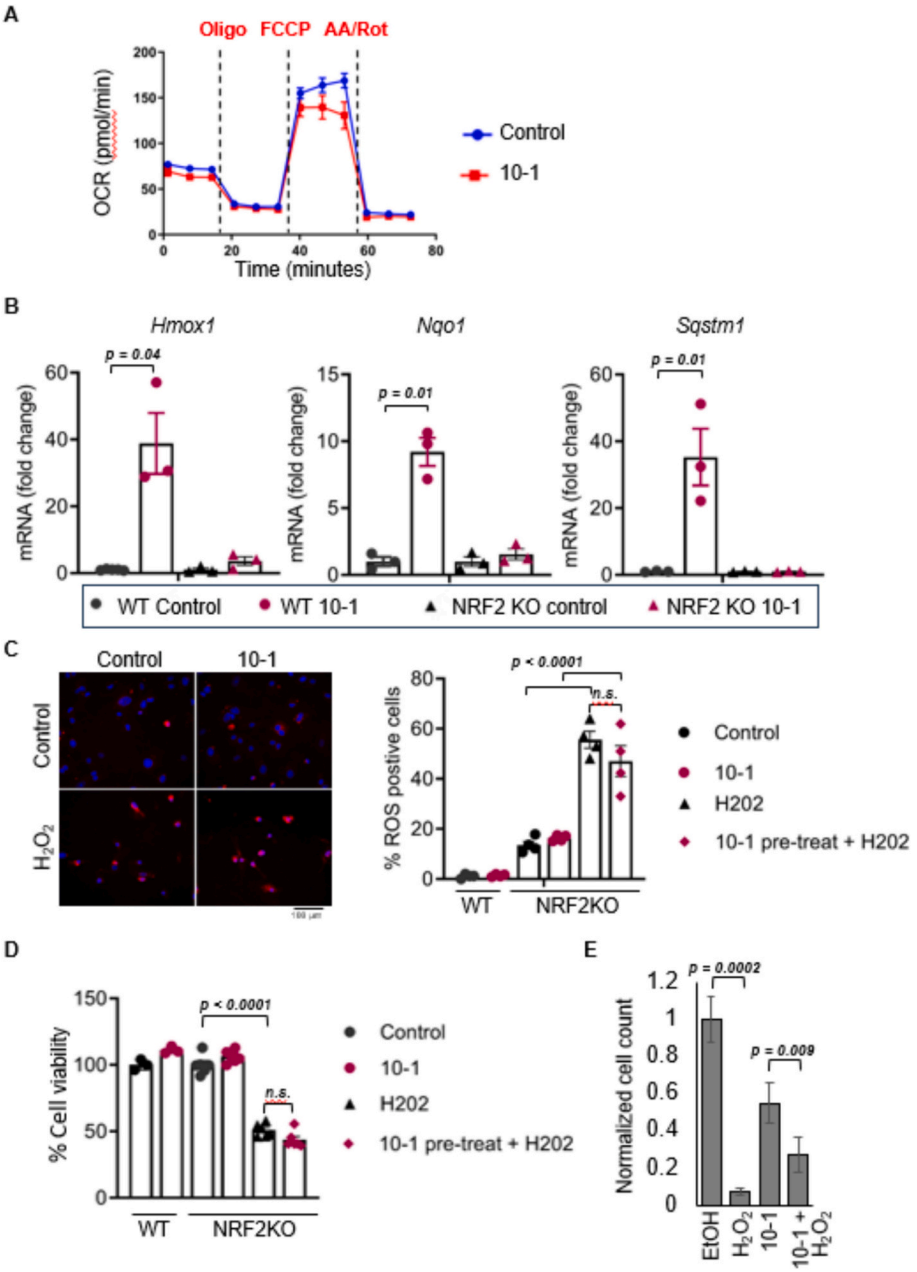

Fig. 6. NRF2 is required for MCB-613-10-1-induced improved mitochondrial function and resistance to oxidative stress. (a) Seahorse analysis of cellular oxygen consumption rate (OCR) in NRF2KO CFs treated with vehicle control compared to MCB-613-10-1 for 24 h. Representative data of three replicate experiments. (b) CFs from NRF2KO mice were treated with vehicle control or MCB-613-10-1 for 24 h. Values shown are mean ± SEM; Student's *t*-test. $n = 3$ for each condition from one of three experiments. (c) NRF2KO CFs were treated with 600 μM H_2O_2 in the presence or absence of MCB-613-10-1 for 24 h. Intracellular ROS was detected using the CellRox assay. Representative images from 3 experiments ($n = 3$ control and $n = 3$ MCB-613-10-1). Quantification of % ROS fluorescence compared to DAPI from 4 images per condition. (d) Cell viability was measured 24 h following addition of 600 μM H_2O_2 with 30-min or 24-h MCB-613-10-1 (6 μM) pre-treatment or co-treatment of H_2O_2 and MCB-613-10-1. Values shown are mean ± SEM; Student's *t*-test. $n = 4$ for each condition from one of two experiments. (e) Cell painting analysis of cellular and mitochondrial features. Quantification of two experiments, $n = 4$ replicates for each experiment. Values shown are mean ± SEM; Student's t-test for H_2O_2 compared to H_2O_2 plus MCB-613-10-1.

1 in response to H_2O_2 treatment (Fig. 5A). Elevated levels of H_2O_2 leads to mitochondrial dysfunction and loss of cell viability in cultured cells [21]. To examine whether MCB-613-10-1 treatment affects cell viability in CFs exposed to oxidative stress, CFs were exposed to H_2O_2 to induce ROS. Cell viability was decreased by 50% following exposure to 600 μM H_2O_2 (Fig. 5B). Pre-treatment of CFs with MCB-613-10-1 for either 30 min or 24-h prevented the decrease in cell viability after H_2O_2 exposure (Fig. 5B), indicating that SRC activation promotes resistance to oxidative stress. Interestingly, MCB-613-10-1 pre-treatment for 24-h increased cell viability in response to H_2O_2, indicating that MCB-613-10-1 enhances the cell adaptive response to oxidative stress. In contrast, MCB-613-10-1 did not inhibit the loss of cell viability following H_2O_2 pre-treatment for 6 h, indicating that MCB-613-10-1 promotes cell survival by controlling the accumulation of intracellular ROS, likely by preserving mitochondrial function.

H_2O_2 exposure can lead to cell death along with mitochondrial fragmentation and mitochondrial dysfunction. We next used Cell Painting to obtain an unbiased assessment of cellular and mitochondrial morphology in response to H_2O_2 and MCB-613-10-1. Cells were stained with fluorescent dyes to detect nuclei (DAPI), nucleoli and cytoplasmic RNA (SYTO-14), F-actin (phalloidin) and mitochondria (MitoTracker) (Fig. 5C). Cell numbers, based on nuclei count, were decreased by 70% following exposure to 900 μM H_2O_2 (Fig. 5C). Pre-treatment of CFs with MCB-613-10-1 for 24-h prevented cell death induced by H_2O_2 exposure (Fig. 5C), indicating that SRC activation promotes resistance to oxidative stress. H_2O_2 altered nuclear eccentricity and actin intensity (Fig. 5C). MCB-613-10-1 reversed the change in nuclear eccentricity indicating that it guards against nuclear abnormalities brought on by H_2O_2 (Fig. 5C). MCB-613-10-1 also rescued the effects of H_2O_2 on nuclear morphology and actin intensity. Next, given that ROS can cause mitochondrial dysfunction and cell death, we specifically looked at the textural characteristics of mitochondria, measured by grey scale correlation matrixes. H_2O_2 robustly changed mitochondrial variance and contrast, indicating the presence of unhealthy mitochondria (Fig. 5D), including promoting mitochondrial network fragmentation [22]. MCB-613-10-1 reversed H_2O_2-induced changes in mitochondrial variance and contrast (Fig. 5D), indicating that MCB-613-10-1 acts as a mitochondrial protectant against oxidative stress-induced mitochondrial damage.

3.5. NRF2 is required for SRC activation mediated cell survival

To determine if NRF2 is required for improved mitochondrial function in response to MCB-613-10-1, oxygen consumption was measured in CFs isolated from NRF2 knock-out (NRF2KO) mice. Unlike WT CFs (Fig. 4E), MCB-613-10-1 did not increase oxygen consumption in NRF2KO CFs (Fig. 6A), indicating NRF2 is required for improved mitochondrial function. To determine if the NRF2/ antioxidant response element (ARE) signaling pathway was involved in the survival of CFs exposed to MCB-613-10-1, NRF2-target gene expression was measured in NRF2KO CFs. SRC expression was not changed in WT CFs compared to NRF2KO CFs indicating that NRF2 is not required for SRC expression (Supplemental Fig. 12). NRF2 was required for transcription of *Hmox1*, *Nqo1*, *Sqstm1* and *Prdx1* antioxidant genes compared to *Gsta3* (Fig. 6B and Supplemental Fig. 12), indicating that the NRF2 transcriptional network is an MCB-613-10-1 therapeutic target in CFs. In support of the transcriptional response, NRF2 was required for HMOX1 protein expression compared to GSTA3 in NRF2KO CFs (Supplemental Fig. 13).

To ascertain if NRF2 is required for MCB-613-10-1 inhibition of ROS production, NRF2KO CFs were exposed to H_2O_2 to induce the generation of intracellular ROS. As shown in previous studies, ROS production is elevated in NRF2KO cells compared to WT CFs [23] (Fig. 6c). MCB-613-10-1 did not inhibit the accumulation of intracellular ROS in response to H_2O_2 treatment (Fig. 6C) indicating NRF2 is required for MCB-613-10-1 inhibition of ROS production. To determine if NRF2 is required for MCB-613-10-1 promotion of CF cell survival, CFs isolated from NRF2KO mice were exposed to H_2O_2 to induce generation of intracellular ROS. As expected, H_2O_2 decreased CF cell survival by 50% 24 h after exposure (Fig. 6D). MCB-613-10-1 did not prevent cell death of NRF2KO CFs indicating that NRF2 is required for MCB-613-10-1 mediated protection against oxidative stress (Fig. 6D).

We next used Cell Painting for the assessment of cellular and mitochondrial morphology in response to H_2O_2 and MCB-613-10-1 in NRF2KO CFs. Cell numbers, based on nuclei count, were decreased by 90% following exposure to 600 μM H_2O_2 (Fig. 6E). Pre-treatment of CFs with MCB-613-10-1 for 24-h resulted in a 50% rescue by MCB-613-10-1 exposure indicating NRF2 is partially required for the anti-apoptotic effect (Fig. 6E). These findings show that NRF2 is required for MCB-613-10-1-mediated increased mitochondrial function, control of accumulation of intracellular ROS and partially required for protection against oxidative stress-induced apoptosis.

3.6. SRC activation enhances antioxidant signaling through interaction with the Hmox1 5′ region

It was previously shown that SRC-3 is required for transcriptional activation of catalase (*Cat*) [24] and is recruited to the promoters of *CAT* [24] and *NRF2* [25] genes.

In HeLa cells, SRC-3 binds in a complex with NRF2 at two AREs upstream of *HMOX1* [25]. We thus wanted to know if SRCs can directly regulate NRF2 signaling in CFs by binding to *Nrf2* ARE sequences in the mouse *Hmox1* gene regulatory region. To identify potential ARE regions in the 5′ of mouse *Hmox1*, we surveyed NRF2-occupied sites in the mouse genome using the publicly available Cistrome Data Browser database (Cistrome.org and [26]). Results from our survey indicate the presence of several potential AREs upstream of mouse *Hmox1* (Supplemental Fig. 14 and Fig. 7A). SRC and NRF2 recruitment to four of these regions, namely potential enhancers E1, E2 and E3, and the promoter P, was tested by qPCR of chromatin immunoprecipitated DNA using anti-SRC-1, 2, 3 or anti-NRF2 antibodies (Fig. 7A). Regions E1, E2 or P1 were not amplified following NRF2 ChIP (data not shown), whereas the E3 ARE sequence was amplified following SRC-1, 2, 3, and NRF2 IP (Fig. 7B) in the absence of MCB-613-10-1, indicating basal enrichment. Interestingly, enrichment of both SRC-1 and NRF2 over E3 was enhanced upon MCB-613-10-1 treatment. These chromatin immunoprecipitation experiments show that SRCs and NRF2 are part of the gene-regulatory network of mouse *Hmox1* in CF, and together with our gene expression data, they suggest that SRC activation stimulates the NRF2 transcriptional network to control cardiac fibroblast antioxidant and cytoprotective signaling. These findings demonstrate the existence of dynamic transcriptional gene regulation of oxidative metabolism by SRCs.

3.7. SRC activation increases HMOX1 expression in cardiac fibroblasts in the core and peri-infarct regions 3 days post-MI

To investigate if SCR stimulation enhances NRF2 activation after MI, we measured HMOX1 in CFs marked by vimentin [27] in hearts from mice treated with control and MCB-613 at 1 day, 3 days and 6 weeks post-MI. HMOX1 was expressed in very few cells 1 day and 6 weeks post-MI (data not shown). In contrast, HMOX1 expression was increased in CFs in the core infarct and per-infarct regions at 3 days post-MI (Fig. 8A) indicating that HMOX1 is temporally expressed in response to injury. SRC activation significantly increased the number and percentage of HMOX1 postive CFs in both the core and pre-infarct regions 3 days post-MI indicating HMOX1 expression is associated with preservation of CFs (Fig. 8B). Remarkably, in response to MCB-613, there was a higher proportion of HMOX1 positive CFs in the core as opposed to the peri-infarct area, suggesting that HMOX1 is linked to slowing the advancement of tissue remodeling. Additionally, SRC activation also increased HMOX1 expression levels in CFs in both the core and peri-infarct regions. Interestingly, HMOX1 expression was more highly expressed in

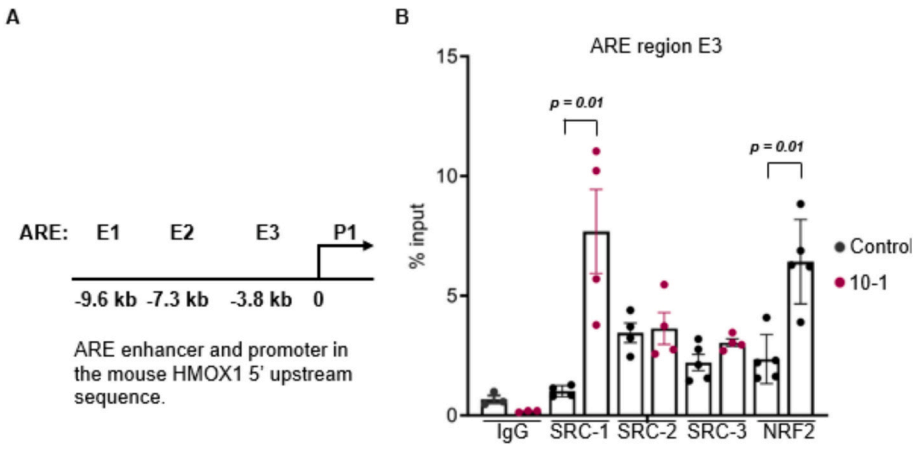

Fig. 7. SRCs-1,2,3 and NRF2 bind to ARE enhancer regions in mouse cardiac fibroblasts. (a) Results from analysis of potential ARE regions in mouse HMOX1 enhancer and promoter regions using the Cistrome.org database. (b) ARE region E2 and E3 were quantified by qPCR in cardiac fibroblasts following IP using IgG, SRC-1,2,3 and NRF2 antibodies. Values shown are mean ± SEM; Student's t-test. $n = 4$ for each condition from one of three experiments.

the CFs in the infarct core (Fig. 8B), suggesting that NRF2 activation in CFs contributes to preventing the progression of cardiac remodeling, most likely by making CFs more resilient to oxidative stress.

4. Discussion

In our previous study, we found that MCB-613 treatment administered after MI, improved cardiac function while preventing the loss of resident CFs and induced a range of CF phenotypic changes during remodeling up to 12 weeks after injury [4]. Here, CF in vitro studies were carried out to identify signaling pathways that are altered in response to the SRC stimulator, MCB-613-10-1, to obtain a mechanistic understanding of CF-derived cardioprotective pathways regulated by SRC stimulation. In our recent animal study, the major cardio protection associated with MCB-613 is its ability to decrease fibrosis, improving cardiac strength and promoting the emergence of a distinct population of cardioprotective fibroblasts that do not express collagen [4]. Thus, although MCB-613 actions coordinate a multifaceted response in vivo, our in vitro findings point to a specific role for SRCs in decreasing fibroblast activation by directly coordinating NRF2 antioxidant signaling in CFs.

Fibroblast activation is an early key response to tissue wounding. In addition to fibroblast activation, we show that SRC activation decreases cytokines and matricellular proteins associated with fibrotic remodeling in CFs, including the inflammatory chemokine CCL2 [28] and the matricellular protein WISP-1 [29]. In addition to their structural function as sentinel cells, fibroblasts are capable of modulating and influencing their surroundings to orchestrate the progression from the initial inflammatory phase to scar tissue maintenance following MI [30]. Our novel finding that SRC activation suppresses expression of secreted ECM remodeling factors including matricellular and lysyl oxidase genes suggests that matricellular proteins provide early and late therapeutic targets that can control cardiac function post MI [31].

Whole transcriptome and proteome analyses of CF-derived signals in response to MCB-613-10-1 revealed that the NRF2 pathway is the dominant activated pathway. The NRF2 transcription factor enables adaptability and survival under stressful conditions by controlling the expression of cytoprotective pathway related genes including those that control antioxidants, anti-inflammatory agents and the repair or removal of damaged macromolecules. There is significant evidence that NRF2 protects against cardiovascular diseases (reviewed in [32]). NRF2-knockout mice, which develop normally [33], are characterized by increased infarct size and decreased cardiac function in response to cardiac injury [32,34]. Here, we show a decrease in KEAP1 protein levels and nuclear accumulation of NRF2 after MCB-613-10-1 treatment. NRF2 is negatively regulated at the protein level by KEAP1 [35]. In the presence of oxidative stress, electrophilic compounds react with cysteine residues on KEAP1 and trigger conformational changes that release NRF2 leading to its stabilization and transcriptional regulation of target genes, including HMOX1. HMOX1 is the rate-limiting enzyme that catalyzes the degradation of pro-inflammatory heme into carbon monoxide and free iron, and biliverdin to bilirubin [36]. We also found robust induction of the key autophagy gene *Sqstm1* after MCB-613-10-1 treatment. Numerous studies have recently found that NRF2 regulates autophagy (reviewed in [37]), potentially linking NRF2 and proteostasis pathways.

We show that the mechanism by which SRC activation enhances the antioxidant response is by SRCs acting as transcriptional coactivators that up-regulate the expression of the *Nrf2* transcriptional network, thereby halting the accumulation of intracellular ROS. Under basal conditions, our results reveal that SRC-1, SRC-2 and SRC-3 all bind AREs in the HMOX1 promoter/enhancer, pointing to their key regulatory roles in supporting homeostatic ROS management in CFs. Increased recruitment of SRC-1 in response to MCB-613-10-1 indicates that SRC-1 enhances NRF2 signaling via interaction with the E3 region of HMOX1. Like SRC-3, as mentioned above, Nrf2 is also known to be critical for anti-inflammatory responses [38,39]. Consistent with our findings, previous studies in cancer cells show that SRC-3 serves as a coactivator for NRF2 [25,40] and the gene encoding for the key antioxidant enzyme catalase [24]. A previous study found that, because of their inability to express catalase, SRC-3 KO macrophages were more susceptible to apoptosis [24]. Taken together, these results indicate direct transcriptional coactivation of NRF2 by MCB-613-10-1 plays a key role in protection against oxidative stress and inflammation.

There is sufficient evidence that antioxidant based therapeutic intervention in animal models can reduce heart damage, prevent fibrosis, and enhance cardiac function [41]. We show that SRC activation promotes cell survival in H_2O_2-treated CFs. This is in line with SRCs well-known function in promoting cell survival in cancer cells by suppressing apoptosis [42]. Here, we demonstrate that SRC activation shields CFs from H_2O_2-induced cell mitochondrial dysfunction and cell death. Interestingly, NRF2 was required for complete rescue of mitochondrial dysfunction and partially required for cell survival, indicating that MCB-613 induces an additional unknown anti-apoptotic pathway. Recently it was discovered that oxidative stress causes synergistic structural and electrical remodeling at the cardiomyocyte-myofibroblasts interface, indicating that reducing fibroblasts adaptive oxidative stress remodeling may enhance cardiac electrical function [43]. Additional evidence in favor of ROS modulation in CFs as a therapeutic target comes from recent work showing that CFs are shielded

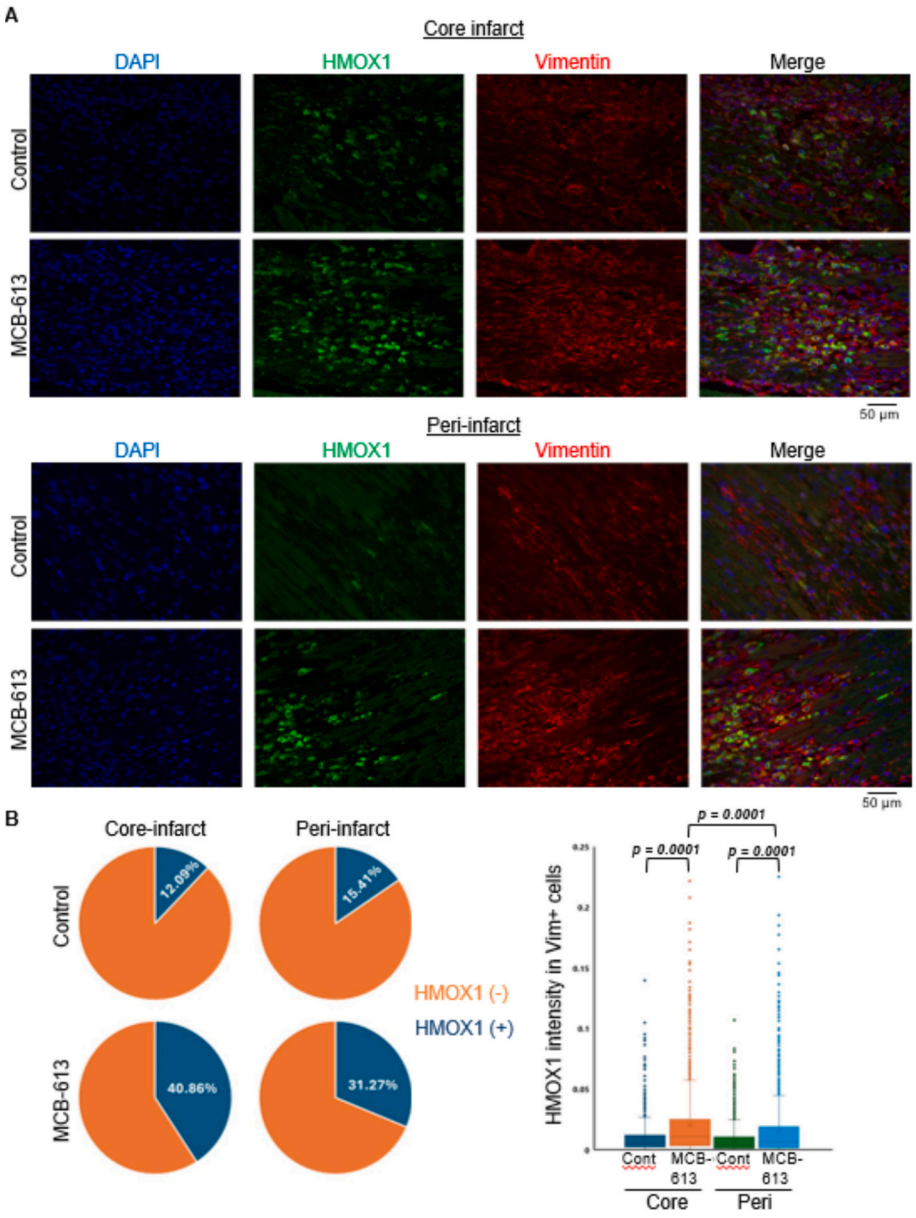

Fig. 8. SRC activation increases HMOX1 expression in cardiac fibroblasts in the core and peri-infarct regions 3 days post-MI. (a) Images of HMOX1, vimentin (CFs) and DAPI staining of core infarct of hearts from mice treated with control or MCB-613. (b) Images of HMOX1, vimentin and DAPI staining of peri- infarct of hearts from mice treated with control or MCB-613. (c) HMOX1 expression in CFs was quantified using CellProfiler in images from 3 fields of view from 3 mice in core infarct and peri-infarct regions.

from post-ischemic activation and proliferation due to the inhibition of ROS accumulation [44]. These findings advance our knowledge of oxidative stress cell survival pathways that can be targeted to improve the ischemic injury response.

Mitochondria, as the major source of chemical energy, are indispensable to processes controlling cell proliferation, differentiation, mitophagy, and cell death as well as helping cells adapt to changing environmental conditions such nutrition and oxygen availability [45–47]. Thus, our studies using freshly isolated 'resident' CFs demonstrate that SRC activation of NRF2 signaling provisions them with an enhanced ability to adapt and survive when exposed to oxidative stress, likely by preventing mitochondrial dysfunction [21,48,49]. Our discovery that SRC activation increases the maximum rate of mitochondrial respiration in CFs suggests that MCB-613-10-1 provides increased adaptability to survive in low oxygen environments, comparable to cancer cells [50]. High respiratory rates in CFs may enable survival in the hypoxic and ischemic conditions following MI, including in the peri-infarct zone. In vivo, HMOX1 expression was robustly induced in CFs at day 3, indicating that MCB-613-10-1 prevents progression of cardiac remodeling in the early phase, consistent with our MI model where we show SRC activation decreases apoptosis, protects against mitochondrial dysfunction and attenuates myofibroblast differentiation 3 days post-MI [4].

Unexpectedly, we observed that pre-treating cells for 24 h with MCB-613-10-1 enhanced their viability. This shows that MCB-613-10-1 might act as a cellular stress pre-conditioning agent with presumed practical utility when ROS is an expected outcome. For example, after exposure to radiotherapy, ROS is a major source of damage to normal tissues, including the skin [51] and ROS are believed to be the principal cause of the anti-tumor drug doxorubicin's cardiotoxic effects [52]. Thus, these findings suggest a paradigm in which SRC activation also may benefit patients' therapeutic outcomes by preventing chemotherapy- or radiotherapy-induced cardiotoxicity or tissue damage.

4.1. Conclusions

These results show that SRC stimulation with MCB-613-10-1 enhances NRF2 antioxidant signaling in CFs to limit the progression of fibrosis. We have demonstrated that SRC activation reduces ECM remodeling factor secretion and gene expression and that this is associated with reduced fibroblast activation. We show that SRC activation directly stimulates the NRF2 pathway, enhances mitochondrial function, prevents accumulation of intracellular ROS and provides resistance to loss of CF cell viability in response to oxidative stress. We found that MCB-613-10-1 protects against ROS-induced mitochondrial dysfunction in CFs. We provide evidence that SRC activation enhances antioxidant and cytoprotective signaling through direct interaction with NRF2. We provide additional evidence showing MCB-613-10-1 decreases KEAP1 protein in the cytoplasm and a corresponding increase of NRF2 in the nucleus. The cooperative activation function by KEAP1 and NRF2 and coactivation function by SRCs likely combine to drive HMOX1 expression in the early remodeling phase post-MI. We discovered that NRF2 is required for the rescue of H_2O_2-induced CF mitochondrial dysfunction and that the MCB-613-10-1 cell survival response involves NRF2 in addition to an unknown anti-apoptotic pathway. These results suggest that MCB-613-10-1's anti-fibrotic and antioxidant properties, by virtue of its upregulation of cytoprotective and antioxidant genes, protects against oxidative damage that ultimately contributes to the robust cardioprotection that we see post-MI with these compounds.

Author contributions

Conceptualization, L.K.M, B.W.O., D.M.L.; Writing-original draft, L. K.M.; Investigation, methodology and formal analysis, L.K.M., D.M.L., B. W.O., C.C·D., R.B.L, K.G., A.P., M.J.B, F.S., M.L. Resources, B.W.O., C.C. D., D.M.L., M.A.M. Writing- review and editing, L.K.M., D.M.L., B.W.O., C.C.D, A.P., R.B.L., M.A.M. Data curation and visualization, L.K.M., R.B. L., K.G., M.J.B., M.L.

Disclosures

Funding has been provided by CoRegen, Inc. to develop SRC small molecule stimulators for clinical use, L.K.M., R.B.L., D.M.L., C.C.D., and B.W.O., A.P., R.B.L.; K.G.

Declaration of generative AI and AI-assisted technologies in the writing process

The authors did not use generative AI or AI-assisted technologies in the development of this manuscript.

Funding statement/Acknowledgements

The authors would like to thank the technical assistance of Colin Peterson for performing cell viability assays and RT-PCR. Imaging for this project was supported by the Integrated Microscopy Core at Baylor College of Medicine and the Center for Advanced Microscopy and Image Informatics (CAMII) with funding from NIH (DK56338, CA125123, ES030285, S10OD030414), and CPRIT (RP150578, RP170719). BCM Mass Spectrometry Proteomics Core is supported by the Dan L. Duncan Comprehensive Cancer Center Award (P30 CA125123), CPRIT Core Facility Awards (RP170005 and RP210227), Intellectual Developmental Disabilities Research Center Award (P50 HD103555), and NIH High End Instrument Award (S10 OD026804, Orbitrap Exploris 480.

CRediT authorship contribution statement

Lisa K. McClendon: Writing – review & editing, Writing – original draft, Validation, Supervision, Methodology, Investigation, Formal analysis, Data curation, Conceptualization. **Rainer B. Lanz:** Writing – review & editing, Software, Methodology, Formal analysis, Data curation. **Anil Panigrahi:** Writing – review & editing, Methodology, Formal analysis, Conceptualization. **Kristan Gomez:** Methodology, Investigation, Formal analysis, Data curation. **Michael J. Bolt:** Software, Resources, Methodology, Investigation, Formal analysis, Data curation, Conceptualization. **Min Liu:** Data curation. **Fabio Stossi:** Formal analysis, Data curation. **Michael A. Mancini:** Supervision, Resources, Methodology, Data curation. **Clifford C. Dacso:** Resources, Funding acquisition. **David M. Lonard:** Writing – review & editing, Supervision, Resources, Funding acquisition. **Bert W. O'Malley:** Writing – review & editing, Supervision, Resources, Methodology, Funding acquisition.

Data availability

Data are available in the Gene Expression Omnibus (GEO) under accession number GSE157542. The mass spectrometry proteomics data have been deposited to the ProteomeXchange Consortium via the PRIDE partner repository with the dataset identifier "PXD050373".

Appendix A. Supplementary data

Supplementary data to this article can be found online at https://doi.org/10.1016/j.yjmcc.2024.07.001.

References

[1] D.M. Lonard, W. O'Malley, Nuclear receptor coregulators: judges, juries, and executioners of cellular regulation, Mol. Cell 27 (5) (2007) 691–700.
[2] R.B. Lanz, et al., Global characterization of transcriptional impact of the SRC-3 coregulator, Mol. Endocrinol. 24 (4) (2010) 859–872.
[3] L.K. Mullany, D.M. Lonard, B.W. O'Malley, Wound healing-related functions of the p160 steroid receptor co-activator family, Endocrinology 162 (3) (2020) 1–11.
[4] L.K. Mullany, et al., A steroid receptor coactivator stimulator (MCB-613) attenuates adverse remodeling after myocardial infarction, Proc. Natl. Acad. Sci. 117 (2020) 3153–31364.
[5] L.K. McClendon, et al., A steroid receptor coactivator small molecule "stimulator" attenuates post-stroke ischemic brain injury, Front. Mol. Neurosci. 15 (2022) 1055295.
[6] M.M. Elahi, Y.X. Kong, B.M. Matata, Oxidative stress as a mediator of cardiovascular disease, Oxidative Med. Cell. Longev. 2 (5) (2009) 259–269.
[7] D. Moris, et al., The role of reactive oxygen species in the pathophysiology of cardiovascular diseases and the clinical significance of myocardial redox, Ann. Transl. Med. 5 (16) (2017) 326.
[8] L. Schirone, et al., A review of the molecular mechanisms underlying the development and progression of cardiac remodeling, Oxidative Med. Cell. Longev. 2017 (2017) 3920195.
[9] Y. Xue, et al., 8-Gingerol ameliorates myocardial fibrosis by attenuating reactive oxygen species, apoptosis, and autophagy via the PI3K/Akt/mTOR signaling pathway, Front. Pharmacol. 12 (2021) 711701.
[10] D.A. Siwik, P.J. Pagano, W.S. Colucci, Oxidative stress regulates collagen synthesis and matrix metalloproteinase activity in cardiac fibroblasts, Am. J. Phys. Cell Phys. 280 (1) (2001) C53–C60.
[11] X. Fu, et al., Specialized fibroblast differentiated states underlie scar formation in the infarcted mouse heart, J. Clin. Invest. 128 (5) (2018) 2127–2143.
[12] A.V. Shinde, N.G. Frangogiannis, Fibroblasts in myocardial infarction: a role in inflammation and repair, J. Mol. Cell. Cardiol. 70 (2014) 74–82.
[13] E. Forte, et al., Dynamic interstitial cell response during myocardial infarction predicts resilience to rupture in genetically diverse mice, Cell Rep. 30 (9) (2020) 3149–3163 e6.
[14] M. Melzer, et al., Isolation and characterization of adult cardiac fibroblasts and myofibroblasts, J. Vis. Exp. 157 (2020).
[15] M.J. Bolt, et al., Systems level-based RNAi screening by high content analysis identifies UBR5 as a regulator of estrogen receptor-alpha protein levels and activity, Oncogene 34 (2) (2015) 154–164.
[16] P. Mertins, et al., Ischemia in tumors induces early and sustained phosphorylation changes in stress kinase pathways but does not affect global protein levels, Mol. Cell. Proteomics 13 (7) (2014) 1690–1704.
[17] K. Nozawa, et al., Testis-specific serine kinase 3 is required for sperm morphogenesis and male fertility, Andrology 11 (5) (2023) 826–839.
[18] C. Rodriguez, J. Martinez-Gonzalez, The role of Lysyl oxidase enzymes in cardiac function and remodeling, Cells 8 (12) (2019).
[19] K.M. Holmstrom, et al., Nrf2 impacts cellular bioenergetics by controlling substrate availability for mitochondrial respiration, Biol. Open 2 (8) (2013) 761–770.
[20] A. Ayer, et al., Heme Oxygenases in cardiovascular health and disease, Physiol. Rev. 96 (4) (2016) 1449–1508.
[21] J. Strom, et al., Nrf2 protects mitochondrial decay by oxidative stress, FASEB J. 30 (1) (2016) 66–80.

[22] S. Wu, et al., Mitochondrial oxidative stress causes mitochondrial fragmentation via differential modulation of mitochondrial fission-fusion proteins, FEBS J. 278 (6) (2011) 941–954.
[23] S. Kovac, et al., Nrf2 regulates ROS production by mitochondria and NADPH oxidase, Biochim. Biophys. Acta 1850 (4) (2015) 794–801.
[24] Q. Chen, et al., Steroid receptor coactivator 3 is required for clearing bacteria and repressing inflammatory response in *Escherichia coli*-induced septic peritonitis, J. Immunol. 185 (9) (2010) 5444–5452.
[25] J.H. Kim, et al., The nuclear cofactor RAC3/AIB1/SRC-3 enhances Nrf2 signaling by interacting with transactivation domains, Oncogene 32 (4) (2013) 514–527.
[26] D.Z. Eichenfield, et al., Tissue damage drives co-localization of NF-kappaB, Smad3, and Nrf2 to direct Rev-erb sensitive wound repair in mouse macrophages, Elife (2016) 5.
[27] S. Liu, et al., Yap promotes noncanonical Wnt signals from cardiomyocytes for heart regeneration, Circ. Res. 129 (8) (2021) 782–797.
[28] M. Dobaczewski, N.G. Frangogiannis, Chemokines and cardiac fibrosis, Front. Biosci. (Schol. Ed.) 1 (2) (2009) 391–405.
[29] K. Venkatachalam, et al., WISP1, a pro-mitogenic, pro-survival factor, mediates tumor necrosis factor-alpha (TNF-alpha)-stimulated cardiac fibroblast proliferation but inhibits TNF-alpha-induced cardiomyocyte death, J. Biol. Chem. 284 (21) (2009) 14414–14427.
[30] G. Diaz-Araya, et al., Cardiac fibroblasts as sentinel cells in cardiac tissue: receptors, signaling pathways and cellular functions, Pharmacol. Res. 101 (2015) 30–40.
[31] Q.J. Zhang, et al., Matricellular protein Cilp1 promotes myocardial fibrosis in response to myocardial infarction, Circ. Res. 129 (11) (2021) 1021–1035.
[32] A. Mata, S. Cadenas, The antioxidant transcription factor Nrf2 in cardiac ischemia-reperfusion injury, Int. J. Mol. Sci. 22 (21) (2021).
[33] K. Chan, et al., NRF2, a member of the NFE2 family of transcription factors, is not essential for murine erythropoiesis, growth, and development, Proc. Natl. Acad. Sci. U. S. A. 93 (24) (1996) 13943–13948.
[34] B. Xu, et al., Myocardial ischemic reperfusion induces de novo Nrf2 protein translation, Biochim. Biophys. Acta 1842 (9) (2014) 1638–1647.
[35] K. Itoh, et al., Keap1 represses nuclear activation of antioxidant responsive elements by Nrf2 through binding to the amino-terminal Neh2 domain, Genes Dev. 13 (1) (1999) 76–86.
[36] S.M. Ahmed, et al., Nrf2 signaling pathway: pivotal roles in inflammation, Biochim. Biophys. Acta Mol. basis Dis. 1863 (2) (2017) 585–597.
[37] Q.M. Chen, A.J. Maltagliati, Nrf2 at the heart of oxidative stress and cardiac protection, Physiol. Genomics 50 (2) (2018) 77–97.
[38] E.H. Kobayashi, et al., Nrf2 suppresses macrophage inflammatory response by blocking proinflammatory cytokine transcription, Nat. Commun. 7 (2016) 11624.
[39] S. Saha, et al., An overview of Nrf2 signaling pathway and its role in inflammation, Molecules 25 (22) (2020).
[40] Q. Chen, et al., Amplified in breast cancer 1 enhances human cholangiocarcinoma growth and chemoresistance by simultaneous activation of Akt and Nrf2 pathways, Hepatology 55 (6) (2012) 1820–1829.
[41] A.M. Rababa'h, et al., Oxidative stress and cardiac remodeling: an updated edge, Curr. Cardiol. Rev. 14 (1) (2018) 53–59.
[42] G. Ma, et al., SRC-3 has a role in cancer other than as a nuclear receptor coactivator, Int. J. Biol. Sci. 7 (5) (2011) 664–672.
[43] Y. Zhao, et al., Proarrhythmic electrical remodeling by noncardiomyocytes at interfaces with cardiomyocytes under oxidative stress, Front. Physiol. 11 (2020) 622613.
[44] V. Janbandhu, et al., Hif-1a suppresses ROS-induced proliferation of cardiac fibroblasts following myocardial infarction, Cell Stem Cell 29 (2) (2022) 281–297 e12.
[45] M. Khacho, et al., Mitochondrial dynamics impacts stem cell identity and fate decisions by regulating a nuclear transcriptional program, Cell Stem Cell 19 (2) (2016) 232–247.
[46] A.J. Molina, et al., Mitochondrial networking protects beta-cells from nutrient-induced apoptosis, Diabetes 58 (10) (2009) 2303–2315.
[47] S. Von Stockum, et al., Mitochondrial dynamics and mitophagy in Parkinson's disease: a fly point of view, Neurobiol. Dis. 90 (2016) 58–67.
[48] C. Bento-Pereira, A.T. Dinkova-Kostova, Activation of transcription factor Nrf2 to counteract mitochondrial dysfunction in Parkinson's disease, Med. Res. Rev. 41 (2) (2021) 785–802.
[49] A.T. Dinkova-Kostova, A.Y. Abramov, The emerging role of Nrf2 in mitochondrial function, Free Radic. Biol. Med. 88 (Pt B) (2015) 179–188.
[50] R.J. DeBerardinis, N.S. Chandel, Fundamentals of cancer metabolism, Sci. Adv. 2 (5) (2016) e1600200.
[51] J. Wei, et al., Radiation-induced skin reactions: mechanism and treatment, Cancer Manag. Res. 11 (2019) 167–177.
[52] E. Christidi, L.R. Brunham, Regulated cell death pathways in doxorubicin-induced cardiotoxicity, Cell Death Dis. 12 (4) (2021) 339.